Journal of Hazardous Materials 163 (2009) 1179–1184

Contents lists available at ScienceDirect

Journal of Hazardous Materials

journal homepage: www.elsevier.com/locate/jhazmat

Preparation and application of visible-light-responsive Ni-doped and SnO_2-coupled TiO_2 nanocomposite photocatalysts

Romana Khan, Tae-Jeong Kim *

Department of Applied Chemistry, Kyungpook National University, Taegu 702-701, Republic of Korea

ARTICLE INFO

Article history:
Received 28 January 2008
Received in revised form 13 June 2008
Accepted 18 July 2008
Available online 25 July 2008

Keywords:
Ni–TiO_2–SnO_2
Nanocomposites
Photocatalytic activity
Visible light

ABSTRACT

A new series of visible-light-driven TiO_2 photocatalysts constituting lattice-doped Ni and surface-coupled SnO_2 nanocomposites, *x*Ni–TiO_2–SnO_2 (*x* = 0.1, 0.3, 0.5), were synthesized. TiO_2 and *x*Ni–TiO_2 were prepared by a sol–gel method while the SnO_2 was coupled to these via a ligand exchange reaction and finally the catalysts were thermally treated. The presence of Ni ions in the lattice of the photocatalysts was indirectly confirmed by a red shift in DRS spectra. XRD showed crystalline peaks only assignable to TiO_2 anatase phase. XPS analysis confirmed that Sn is present on the surface of the catalysts as SnO_2 while Ni_2O_3 is absent. The *x*Ni–TiO_2–SnO_2 nanocomposites showed a promising visible-light-responsive photocatalytic activity and were found superior to TiO_2, *x*Ni–TiO_2 and TiO_2–SnO_2 for the degradation of toluene in air.

1. Introduction

Titanium oxide (TiO_2) is one of the most efficient semiconductor photocatalysts for extensive environmental applications because of its strong oxidizing power, non-toxicity, high photochemical corrosive resistance and cost effectiveness. Due to these inherent properties, TiO_2 is the most suitable candidate for degradation and complete mineralization of toxic organic pollutants in water, soil and air [1–4]. Yet, the widespread technological use of TiO_2 is impaired by its wide band gap (3.2 eV for crystalline anatase phase) which requires the use of UV light. Thus, the possibility of employing solar light in TiO_2 photocatalysis is limited. It is noteworthy that the UV-radiation fraction of the global solar radiation is only 4–6% while its visible light component is 45% [5]. Therefore, development of an efficient process that can shift the optical response of TiO_2 from the UV to visible spectral range seems to be the most appropriate strategy to improve the photocatalytic efficiency of TiO_2 under solar light irradiation [6].

Among others, the substitution of Ti by transition metals through doping is the most widely studied approach for the synthesis of visible-light-active photocatalysts [7–10]. However, unlike other metals, there have been relatively few studies on Ni doping into TiO_2 lattice for photocatalytic degradation of organic pollutants [8]. Nevertheless, Ni^{2+} has been found to be an efficient dopant for improving the photocatalytic activity of certain semiconductor photocatalyst for hydrogen evolution from water [11]. In principle, transition metal with proper oxidation state replace some of the Ti(IV) from lattice producing a impurity state that reduces the band gap of TiO_2 [8,12]. However, metal doping has some drawbacks, the most crucial of which is that the doped metal centers act as electron traps, which ultimately results in higher rate of electron and hole pairs (e^-/h^+) recombination [13]. Therefore, further studies are required in order to improve the activity of these transition-metal-doped TiO_2 by holding back the possible accumulation of electrons on TiO_2. This will in turn suppress the recombination of photogenerated e^-/h^+ and thus will improve the efficiency of the net charge transfer in photocatalysis. Coupling of two semiconductor particles with different Fermi levels provides an interesting approach in this regard. The TiO_2–SnO_2 system seems to be a pair of choice because of the structural analogy between both oxides. The band gaps of SnO_2 and TiO_2 are 3.8 and 3.2 eV, respectively. When these two semiconductor particles are coupled, the conduction band of SnO_2 acts as a sink for photogenerated electrons. Since the photogenerated holes move in the opposite direction, they accumulate in the valence band of the TiO_2 particle, therefore, leading to efficient spatial separation of photogenerated charges and thus suppressing recombination [14,15].

Several methods ranging from thin films and particles to nanofibers have been developed to produce TiO_2–SnO_2 materials [16–18]. Such a combination is certainly advantageous but can be active only under UV light. Substitution of Sn for Ti in a TiO_2 lattice matrix can only bring a blue shift in the absorption spectra of TiO_2 because SnO_2 have a large band gap than TiO_2. Therefore, it

* Corresponding author. Tel.: +82 539505587; fax: +82 539506594.
E-mail address: tjkim@knu.ac.kr (T.-J. Kim).

0304-3894/$ – see front matter © 2008 Elsevier B.V. All rights reserved.
doi:10.1016/j.jhazmat.2008.07.078

seems crucial for visible light activity that there should be a surface coupling between the two semiconductors.

The aim of the present study was to change the response of TiO_2 from UV to visible light irradiations by doping with nickel and to improve the efficiency of mix–metal system by coupling it with SnO_2 semiconductor. The uniqueness of the system is while Ni is introduced at atomic level to replace Ti in the lattice, SnO_2 is coupled to TiO_2 only on the surface.

2. Experimental

2.1. General remarks

All commercial reagents such as tetrabutyl titanate, nickel chloride, triphenyltin hydroxide, absolute ethanol, hydrochloric acid (37%) and ammonium hydroxide (28%) were purchased from Aldrich and used as received. All syntheses were carried out using deionized water and under nitrogen at room temperature. TiO_2 was prepared according to the literature method described elsewhere [19].

2.2. Preparation of Ni-doped TiO_2

Ni-doped TiO_2 and xNi–TiO_2 (x = 0.1, 0.3, and 0.5 wt%) were prepared initially by taking advantage of a modified sol–gel method [19]. In a typical experiment for the synthesis of 0.1 wt% Ni–TiO_2, to a stirred solution of $Ti(OBu)_4$ (21.3 mL) in EtOH (120 mL) charged in a two-neck round bottom flask, were added dropwise a solution of HCl (6.6 mL) in aqueous ethanol (22:120 v/v). Simultaneously was added dropwise a solution of $NiCl_2{\cdot}6H_2O$ (0.02 g) in ethanol (30 mL). After addition, the resulting sol was stirred for an additional 24 h and subsequently the pH of the solution was raised to 9.0 by dropwise addition of NH_4OH (1.0 M) solution. The gel thus formed was aged for 2 h, filtered and washed thoroughly with distilled water for the complete removal of chlorides as confirmed by silver nitrate test. The gel was then dried at 110 °C for 12 h and mechanically ground to powder. The resulting dry powders were calcined at 500 °C at the rate of 1 °C/min and kept at 500 °C for 5 h to obtain nanostructured TiO_2 powders. Those with other Ni-contents such as 0.3 and 0.5 wt% Ni–TiO_2, were prepared in the same manner.

2.3. Preparation of xNi–TiO_2–SnO_2 and TiO_2–SnO_2

A series of xNi–TiO_2–SnO_2 with various Ni-contents (x = 0.1, 0.3, and 0.5 wt%) was prepared using wet-impregnation method; namely, xNi–TiO_2 (4 g prior to calcination) was added to an ethanolic solution of $(C_6H_5)_3Sn$–OH (0.12 g). After stirring for 6 h followed by aging for 24 h, the suspension obtained was centrifuged and the residue was washed with distilled water. Then, it was dried to obtain the powdered product which was calcined to 500 °C at the rate of 1 °C/min and kept at 500 °C for 5 h to obtain xNi–TiO_2–SnO_2.

TiO_2–SnO_2 was also prepared in the same manner except xNi–TiO_2 was replaced with TiO_2.

2.4. Characterization

The UV–vis diffuse reflectance spectra were measured by using a SHIMADZU UV-2450 spectrophotometer. The crystallite structures of the calcined (at 500 °C) materials were investigated by analyzing the X-ray diffraction (XRD) patterns obtained with a Multi-Purpose X-ray Diffractometer (X'pert PRO MRD/X'pert PRO MPD) operated at room temperature with graphite-monochromated Cu Kα radiation. The Scherrer's formula

$$\text{Crystallite size} = \frac{k\lambda}{W}\cos\theta \quad (1)$$

(with a shape factor k = 0.89) was employed to determine the crystallite sizes of samples with fwhms (W) and peak centers obtained by fitting the (1 0 1) peak to the Lorentzian function; here λ is the wavelength of X-ray radiation (1.54 Å). The lattice parameters of the catalysts were measured using (1 0 1) and (2 0 0) in anatase crystal planes by using the following equations:

$$\text{Bragg's equation}: \quad d_{hkl} = \frac{\lambda}{2\sin\theta} \quad (2)$$

$$\text{Formula for tetragonal system}: d_{hkl}^{-2} = h^2a^{-2} + k^2b^{-2} + l^2c^{-2} \quad (3)$$

where d_{hkl} is the distance between crystal planes of ($h\,k\,l$), λ is the X-ray wavelength, θ is the diffraction angle of crystal plane ($h\,k\,l$), $h\,k\,l$ is the crystal index, and a, b and c are lattice parameters (in anatase form, $a = b \neq c$). X-ray photoelectron spectra (XPS) were recorded on a VG Microtech, MT 500/1 photoelectron spectrometer. All the binding energies were referenced to the adventitious C 1s peak at 285 eV.

2.5. Measurement of photocatalytic activity

The photocatalytic activity was investigated by the photodegradation of gaseous toluene under visible light irradiation using a closed circulation reactor (batch type reactor) at ambient condition. A Pyrex-glass tubular reactor, containing the catalyst (300 ± 0.5 mg) uniformly spread over the irradiation area was connected to a peristaltic pump through tubing.

The reactor containing the catalyst was placed in a black glass box (30 cm × 42 cm × 27 cm) that housed a 150-W halogen lamp (OSRAM HALOLINE) with a 400 nm cutoff filter as a visible light source. The photon flux emitted from this lamp was determined actinometrically using the potassium ferrioxalate method and was found to be 3.9×10^{-6} Einstein/s. The quantum yield was determined using the following equation as described elsewhere [20].

$$\Phi = \frac{(dC_0/dt)V_T}{I_0} \quad (4)$$

where dC_0/dt is the degradation rate (mol/dm^3 min), V_T is the total system volume (dm^3) and I_0 is the amount of photons entering the photocatalytic reaction zone (Einstein/s).

The distance between the lamp and the catalyst was 15 cm. To introduce toluene for photodegradation study, the reactor was connected to a glass-mixing chamber, where the temperature was maintained at 70 °C to ensure the vaporization of toluene. A Master Flex peristaltic pump and tubing was used to homogenize the gas inside the reactor. The pump constantly circulated the gas inside the reactor with a flow rate of 320 cm^3/min. This ensured both the gas mixing and maintenance of the gaseous concentration of the vaporized toluene to the catalysts. The total volume of the circulation reactor was 1.3 L. The concentration of toluene used in all experiments was 177 ppm, using a volume of 1.0 μL. The photoreactor was kept in the dark and the gas was circulated for one hour during which the gas concentration became constant as monitored by GC. This indicated that the gaseous toluene achieved a steady state between adsorption and desorption on the catalyst surface. No considerable loss of toluene was observed during the experiments as determined by taking various blanks such as: (i) without catalyst and visible light, (ii) with catalyst but without visible light displayed. In order to monitor the concentration of toluene versus time, a Gas Chromatograph (Shimadzu GC-17A) equipped with a gas sampler operating with a flame ionization detector (FID) was connected to the reactor. The rate of degradation was estimated to

obey pseudo-first-order kinetics and hence the rate constant for degradation, k, was obtained from the first-order plot according to Eq. (5).

$$\ln\left(\frac{C_0}{C}\right) = kt \quad (5)$$

where C_0 is the initial concentration, C is the concentration after a time (t) of the toluene degradation, and k is the first-order rate constant.

3. Results and discussion

3.1. Synthetic process

Quantitative incorporation of a dopant metal into TiO_2 lattice is feasible provided dopant metal ions have the same ionic radius as that of Ti^{4+} (0.75 Å) [8]. In the sol–gel process the incorporation of active ions in the sol allows the ions to have direct interaction with TiO_2 and could be doped into the lattice of TiO_2. The resulting materials will have special optical and catalytic properties [5]. This means that the Ni^{2+} ions having the same ionic radius as that of Ti^{4+} can successfully replace some of the Ti^{4+} ions from lattice through doping using sol–gel method. This process results in the formation of a mix–metal system of Ni–TiO_2 having different optical and catalytic properties than the parent TiO_2.

TiO_2 has a large number of highly reactive dandling bonds –OH on its surface [2]. Triphenyltin hydroxide, used as a precursor in the present study, is a bulky compound containing –OH bond. Therefore, it is possible that ligand exchange takes place between the dandling bonds and triphenyltin hydroxide. Due to attached bulky organic groups it is impossible for Sn^{4+} to exist as solid solution or replace Ti^{4+}. When annealed at 500 °C, the precursor takes a thermal decomposition and the organic ligands are oxidized and vaporized. It is worth noting that under the applied conditions the carbon of the organic component fully oxidized to CO_2 which is comparatively less toxic. The oxide remained on the surface is SnO_2 coupled with TiO_2.

3.2. UV–vis absorption spectra

Fig. 1 shows the UV–Vis spectra of TiO_2, xNi–TiO_2, and, xNi–TiO_2–SnO_2. The significant increase in the absorption at a wavelength lower than 380 nm (ca. 3.18 eV) can be assigned to the intrinsic band gap absorption of anatase TiO_2. SnO_2-coupled TiO_2 showed blue shift obviously due to a larger band gap of SnO_2 (3.8 eV) compared to TiO_2 (3.2 eV). The absorption edge of TiO_2 shifts towards longer wavelength after Ni doping (Fig. 1). Furthermore, such a red shift depends linearly on the Ni content. These observations showed that the absorption edge of TiO_2 can be engineered towards longer wave length by introduction of Ni into lattice of TiO_2. Similar trend was also observed for xNi–TiO_2–SnO_2 samples. Compared to SnO_2-coupled TiO_2 which induces a blue shift, xNi–TiO_2–SnO_2 causes a red shift probably due to the presence of Ni ions inside lattice thus causing higher influence than surface-coupled SnO_2. The change in the red shift was of the following order: TiO_2–SnO_2 < TiO_2 < 0.1 wt% Ni–TiO_2–SnO_2 < 0.1 wt% Ni–TiO_2 < 0.3 wt% Ni–TiO_2 ~ 0.3 wt% Ni–TiO_2–SnO_2 < 0.5 wt% Ni–TiO_2 ~ 0.5 wt% Ni–TiO_2–SnO_2.

3.3. XRD analysis

Fig. 2 shows the XRD patterns of xNi–TiO_2, xNi–TiO_2–SnO_2 and TiO_2–SnO_2. All diffraction peaks can be assigned as pure anatase TiO_2 after calcinations. These observations indicated that there has been virtually no phase change in TiO_2 in the process of doping, regardless of the type and amount of dopants. Segregation appears as a separate phase in the XRD analysis as reported previously [21]. In Contrast, no segregate phase was found for SnO_2 in the XRD pattern and thus most probably SnO_2 distributes uniformly on the surface of TiO_2. This postulation was confirmed by the XPS analysis of these samples. No segregate phase was found for SnO_2 and thus most probably SnO_2 distributes uniformly on the surface of TiO_2. Table 1 reveals the estimated lattice parameters and crystallite sizes. The lattice parameters for all Ni–TiO_2 samples remain almost unchanged along a- and b-axes, whereas the c-axis parameter showed a slight increase with Ni-doping. This increase may be due to the compensating effects between substitution of Ti(IV) by the dopant Ni(II) in the lattice and due to oxygen vacancy formation for maintenance of charge neutrality [22,23]. For SnO_2–TiO_2-coupled system the lattice parameters remained unchanged indicating that no substitution has taken place at lattice of TiO_2.

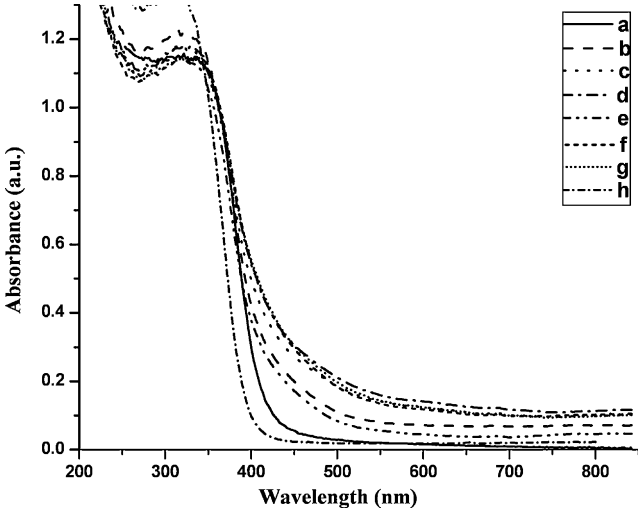

Fig. 1. DRS of (a) TiO_2; (b) 0.1 wt% Ni–TiO_2; (c) 0.3 wt% Ni–TiO_2; (d) 0.5 wt% Ni–TiO_2; (e) 0.1 wt% Ni–TiO_2–SnO_2; (f) 0.3 wt% Ni–TiO_2–SnO_2; (g) 0.5 wt% TiO_2–SnO_2; and (h) 1 wt% TiO_2–SnO_2.

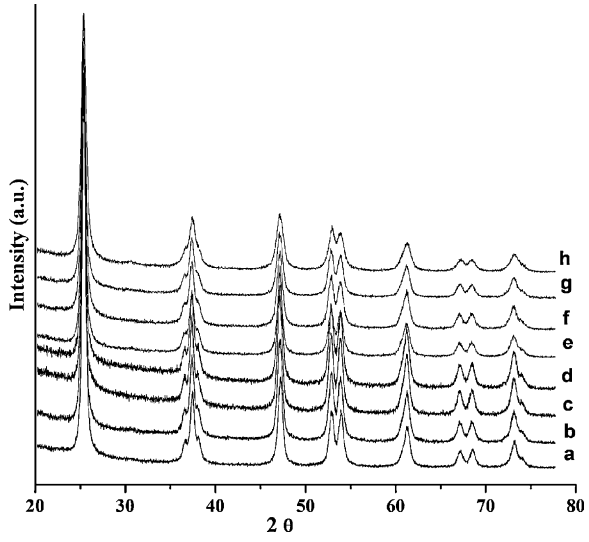

Fig. 2. XRD analysis of (a) TiO_2; (b) 0.1 wt% Ni–TiO_2; (c) 0.3 wt% Ni–TiO_2; (d) 0.5 wt% Ni–TiO_2; (e) 0.1 wt% TiO_2–SnO_2; (f) 0.3 wt% TiO_2–SnO_2; (g) 0.5 wt% TiO_2–SnO_2; and (h) 1 wt% TiO_2–SnO_2.

Table 1
Lattice parameters, average crystallite size, rate constant and quantum yield of xNi–TiO_2, xNi–TiO_2–SnO_2, TiO_2, and TiO_2–SnO_2.

Catalysts	Lattice parameters (Å)[a]		Crystallite size (nm)[b]	K[c] (min^{-1})	ϕ[d]
	$a=b$	c			
TiO_2	3.7874	9.4067	18	0.0007	0.02
0.1 wt% Ni–TiO_2	3.7820	9.4913	18	0.0039	0.15
0.3 wt% Ni–TiO_2	3.7834	9.5006	18	0.0033	0.12
0.5 wt% Ni–TiO_2	3.7834	9.5149	18	0.0014	0.07
0.1 wt% Ni–TiO_2–SnO_2	3.7850	9.4447	16	0.0036	0.11
0.3 wt% Ni–TiO_2–SnO_2	3.7825	9.4840	16	0.0058	0.18
0.5 wt% Ni–TiO_2–SnO_2	3.7829	9.4765	15	0.0026	0.11
SnO_2–TiO_2	3.7811	9.4118	13	0.0003	0.02

[a] Estimated according to Eqs. (2) and (3).
[b] Calculated according to the Scherrer formula ($D = k\lambda/B\cos\theta$).
[c] Calculated from linear fitting of $\ln(C_0C)$ versus the reaction time.
[d] Calculated according to Eq. (4).

Table 1 shows that the average crystallite size of the catalysts did not change with the Ni doping possibly due to the very small quantity of Ni added as a dopant. On the other hand, in xNi–TiO_2–SnO_2 series the presence of SnO_2 (1 wt%) on the surface retarded the crystal growth. Thus these samples showed a decrease in crystalline size from parent TiO_2 as well as xNi–TiO_2. This effect was more pronounced in TiO_2–SnO_2, where the crystallite size was 13 nm as compared to TiO_2 (18 nm) (Table 1).

3.4. XPS analysis

XPS is a highly sensitive technique of surface analysis, and is an effective method to investigate the surface composition and chemical states of solid samples. XPS measurements were carried out to determine the surface composition and chemical state of 0.5 wt% Ni–TiO_2–SnO_2 calcined at 500 °C. The XPS survey spectrum in Fig. 3 demonstrates the presence of titanium, oxygen, carbon, and tin, and

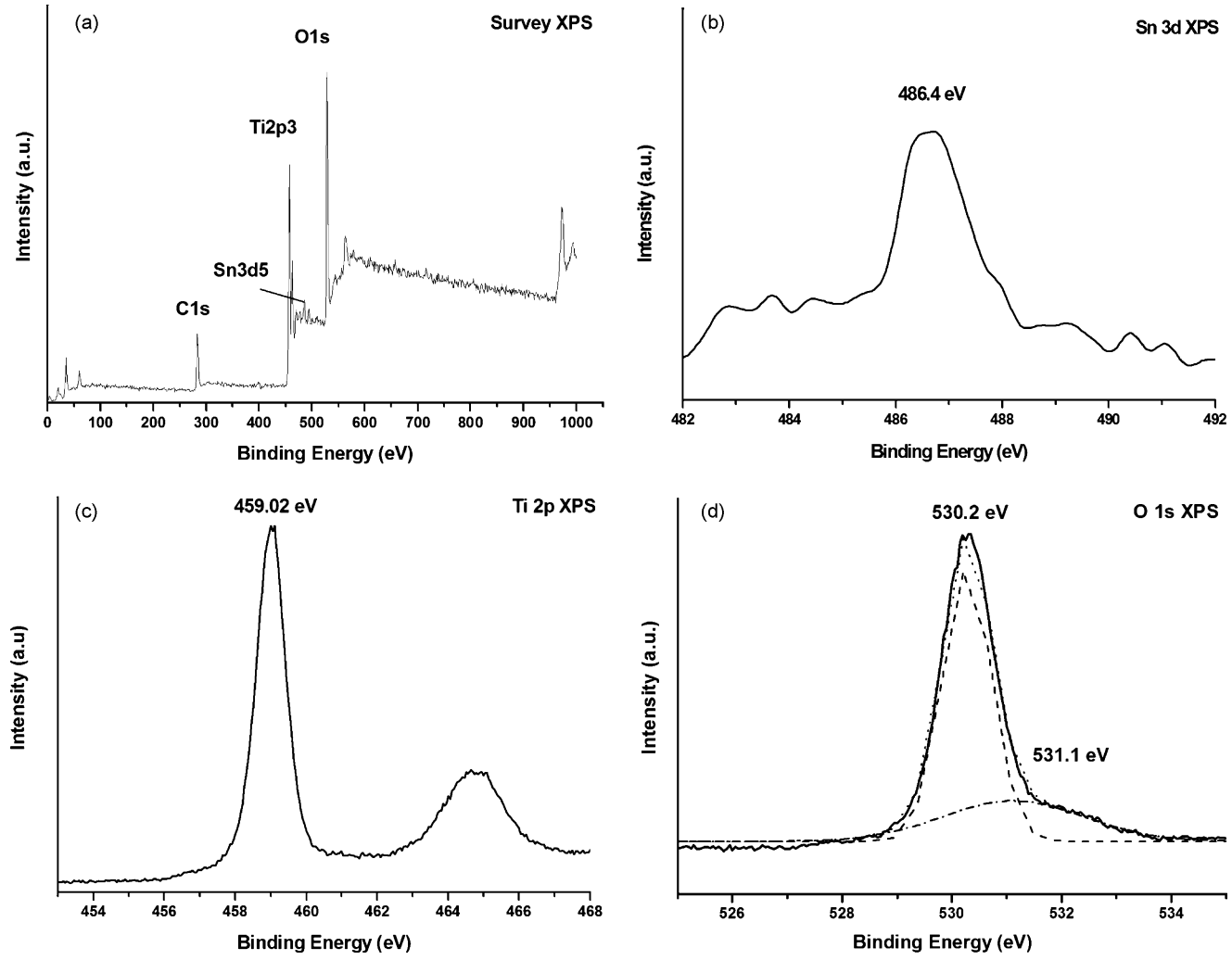

Fig. 3. XPS analysis of calcined 0.5 wt% TiO_2–SnO_2: (a) survey analysis; (b) Sn (3 d); (c) Ti (2p); (d) O (1s).

at the same time the absence of nickel on the surface. All the binding energies were referenced to the adventitious C 1s peak at 284.6 eV.

The XPS peak position of Ti $2p_3$ and Sn $3d_5$ are at 459.02 and 486.4 eV, respectively, demonstrating that the main chemical states of Ti and Sn are +4 valence according to the handbook of XPS instrument. The O 1s XPS spectrum can be resolved into two components using Origin software with Gaussian rule. Both O 1s XPS peaks are wide and asymmetric demonstrating that there are at least two kind of O binding states. The one at 530.2 eV is assignable to the crystal lattice oxygen (Ti–O, Sn–O) and the other hydroxyl oxygen (OH) at 531.1 eV to adsorbed O_2/OH groups on the surface. The atomic percent determined from XPS analysis shows carbon 21.3%, oxygen 55.72%, titanium 22.22% and tin 0.76%. The content Sn on the surface is close to the desired content (1%), illustrating that Sn is uniformly dispersed in the TiO_2 sample. In general, for an ideal TiO_2 crystal the ratio of Ti to O is 1:2. Here, we found that the content of oxygen is higher than this ratio which may be due to Sn-bound oxygen. Furthermore, no XPS peak was found in the region 840–890 eV that could be assigned to Ni $2p_3$ clearly indicating that nickel is not present on the surface of TiO_2.

3.5. Photocatalytic activity

The photocatalytic degradation of toluene under visible light irradiation was performed in order to benchmark the catalytic activity of *x*Ni–TiO_2, *x*Ni–TiO_2–SnO_2, TiO_2 and TiO_2–SnO_2. All reactions followed pseudo first-order kinetics as the rate of reaction depends only on toluene concentration while the amount of TiO_2 (catalyst) is fixed and remained unchanged. A straight line was obtained when $\ln C_0/C$ was plotted against time (data not shown). Table 1 describes the rate constants (K) for each reaction. The rate constant for 0.3 wt% Ni–TiO_2–SnO_2 was found to be highest (0.0058 min^{-1}) among the tested catalysts. All samples exhibited varying degrees of catalytic activity depending on the nature of doping. *x*Ni–TiO_2 were found to be active in visible light while coupling of SnO_2 onto the TiO_2 surface further increased the efficiency of these catalysts. The optimum concentration of metal dopant has been found to be the most the crucial factor in determining the efficiency of the TiO_2 photocatalyst [13,24,25]. Metal concentration below the optimum level leads to lower absorption of light while at higher concentration the dopant act as electron–hole recombination center which increase the recombination rate. Both these situations yield lower photocatalytic efficiency. In the present study, the 0.3 wt% Ni–TiO_2–SnO_2 was found to be the best catalyst in the series having the highest quantum yield of 0.18 (Table 1 and Fig. 4). According to DRS analysis, both *x*Ni–TiO_2 and *x*Ni–TiO_2–SnO_2 series showed a red shift in the absorption spectra of TiO_2 due to the presence of Ni ions inside lattice. Furthermore, such a red shift was dependent on the Ni content (Fig. 1). It is evident from the results that 0.3 wt% Ni–TiO_2–SnO_2 absorbed more visible light than 0.1 wt% Ni–TiO_2–SnO_2 and thus displayed better photocatalytic activity. However, when the Ni concentration was further increased to 0.5 wt%, no significant difference in the visible light absorption was observed. Moreover, Ni^{2+} in higher concentrations may act as recombination center for photogenerated electron–hole pairs. Therefore, the photocatalytic efficiency decreased beyond 0.3 wt% Ni concentration in the Ni–TiO_2–SnO_2 series.

The 0.1 wt% Ni–TiO_2 showed good photocatalytic activity, however, the reactivity decreased sharply beyond this concentration (Fig. 4). It has been reported that with the increase in Ni content as dopant it acts as a recombination center [13] and could also be the possible reason for the decrease in activity beyond 0.1 wt% in the present study. The electron and hole pairs formed can soon recombine generating only heat instead of participating in the oxidation reaction. However, when Ni-doped TiO_2 nanoparticles host SnO_2

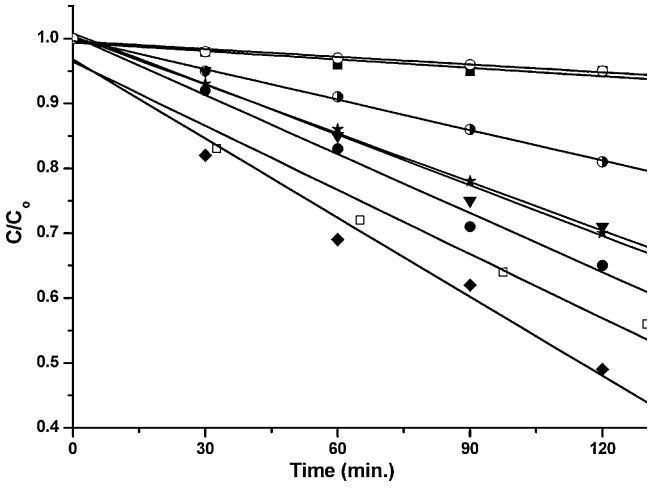

Fig. 4. Degradation of toluene under visible light irradiations: 0.1 wt% Ni–TiO_2 (□); 0.3 wt% Ni–TiO_2 (●); 0.5 wt% Ni–TiO_2 (◑); 0.1 wt% Ni–TiO_2–SnO_2 (▼); 0.3 wt% Ni–TiO_2–SnO_2 (♦); 0.5 wt% Ni–TiO_2–SnO_2 (⋆) TiO_2 (■); Sn–TiO_2 (○).

on their surface, the recombination is retarded. Consequently, it can be seen from the results that all Ni–TiO_2–SnO_2 samples are photocatalytically more active than the corresponding Ni–TiO_2 samples (Table 1 and Fig. 4). The SnO_2 on the surface of Ni–TiO_2 act as a sink for photogenerated electrons. Though the band gap of SnO_2 is wider than that of TiO_2, its conduction band is at a lower energy level than that of TiO_2 (Fig. 5). Hence, in coupled TiO_2–SnO_2, it could be expected that the photogenerated electrons from TiO_2 are transferred easily into the SnO_2, $(TiO_2)e^-_{CB} \rightarrow (SnO_2)e^-_{CB}$ and the holes flow oppositely. One of the noticeable characteristics of TiO_2 is that the oxidizing power of the holes is greater than the reducing power of the excited electrons [26], which is now available to attack surface adsorbed species. Once separated, both the electrons and the holes can be more involved in interfacial charge transfer reaction. The expected key reactions for the investigated photocatalytic system are as follows:

$$Ni\text{–}TiO_2 \rightarrow h_{vb}^{+} + e_{cb}^{-}$$

$$(TiO_2)e_{cb}^{-} \rightarrow (SnO_2)e_{cb}^{-}$$

$$[(SnO_2)e_{cb}^{-}] + O_2 \rightarrow {}^{\bullet}O_2^{-}$$

$$H_2O + h_{vb}^{+} \rightarrow {}^{\bullet}OH + H^{+}$$

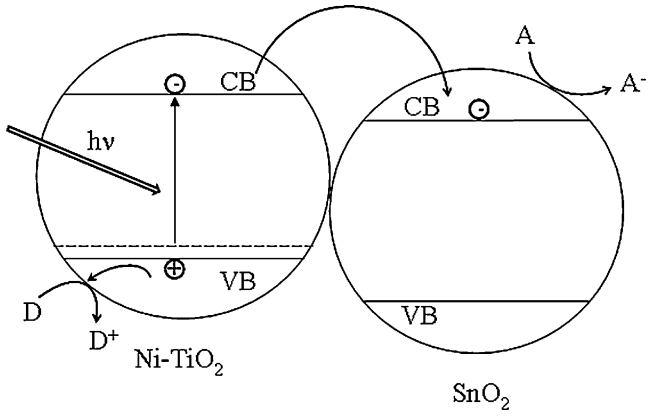

Fig. 5. The schematic diagram for proposed electronic transition for Ni–TiO_2–SnO_2.

TiO_2 as well as TiO_2–SnO_2 were found inactive under visible light irradiations. The lack of activity can be explained in terms of large band gap of the two catalysts as determined by diffuse reflectance spectra of the samples (Fig. 1).

4. Conclusion

A new visible-light-responsive photocatalytic system employing TiO_2 nanoparticles, with Ni^{2+} in the lattice and Sn^{4+} on the surface, was successfully prepared by a sol–gel method followed by a ligand exchange reaction and finally thermal treatment. *x*Ni–TiO_2–SnO_2 samples were photocatalytically more superior to the corresponding *x*Ni–TiO_2 under visible light. The surface coupling of SnO_2 to TiO_2 acted as a sink for the photogenerated electrons and thus decreased the electron–hole pair recombination rate and subsequently improved the photocatalytic activity of the TiO_2 under visible light irradiation. This newly developed photocatalytic system has enormous potential applications in the deep mineralization of recalcitrant organics by avoiding the accumulation of electrons on metal oxide semiconductors. Moreover, with this system in hand, solar light can be used as the most available and cost effective energy source for practical applications. Overall, the lattice-doped metal and surface-coupled semiconductor system developed in the present study proved to be a promising tool for the photodegradation of toluene under visible light.

Acknowledgements

Financial support from Korea Institute of Construction & Transportation Technology Evaluation and Planning (grant no. C10A1000018-06A0200-01220) is acknowledged. R. Khan acknowledges financial support from KRF (KRF-2006-211-C00038).

References

[1] M.A. Fox, M.T. Dulay, Heterogeneous photocatalysis, Chem. Rev. 93 (1993) 341–357.
[2] M.R. Hoffmann, S.T. Martin, W. Choi, D.W. Bahnemann, Environmental applications of semiconductor photocatalysis, Chem. Rev. 95 (1995) 69–96.
[3] A. Fujishima, T.N. Rao, D.A. Tryk, Titanium dioxide photocatalysis, J. Photochem. Photobiol. C: Photochem. Rev. 1 (2000) 1–21.
[4] P. Saritha, C. Aparna, V. Himabindu, Y. Anjaneyulu, Comparison of various advanced oxidation processes for the degradation of 4-chloro-2-nitrophenol, J. Hazard. Mater. 149 (2007) 609–614.
[5] X. Yang, C. Cao, K. Hohn, L. Erickson, R. Maghirand, D. Hamal, K. Klabunde, Highly visible-light active C- and V-doped TiO_2 for degradation of acetaldehyde, J. Catal. 252 (2007) 296–302.
[6] H. Irie, Y. Watanabe, K. Hashimoto, Nitrogen-concentration dependence on photocatalytic activity of $TiO_{2-x}N_x$ powders, J. Phys. Chem. B 107 (2003) 5483–5486.
[7] A.K. Ghosh, G.P. Maruska, Photoelectrolysis of water in sunlight with sensitized semiconductor electrodes, J. Electrochem. Soc. 24 (1977) 1516–1522.
[8] W. Choi, A. Termin, M.R. Hoffmann, The role of metal-ion dopants in quantum-sized TiO_2: correlation between photoreactivity and charge-carrier recombination dynamics, J. Phys. Chem. 98 (1994) 13669–13679.
[9] M. Anpo, Photocatalysis on titanium oxide catalysts: approaches in achieving highly efficient reactions and realizing the use of visible light, Catal. Surv. Jpn. 1 (1997) 169–179.
[10] R. Khan, S.W. Kim, T.-J. Kim, Synthesis and control of physical properties of titania nanoparticles as a function of synthetic parameters, J. Nanosci. Nanotechnol. 8 (2008) 1–5.
[11] D. Jing, Y. Zhang, L. Guo, Study on the synthesis of Ni-doped mesoporous TiO_2 and its photocatalytic activity for hydrogen evolution in aqueous methanol solution, Chem. Phys. Lett. 415 (2005) 74–78.
[12] T. Umebayashi, T. Yamaki, H. Itoh, K. Asai, Analysis of electronic structure of 3d transition metal doped TiO_2 based on band calculations, J. Phys. Chem. Solids. 63 (2002) 1909–1920.
[13] S. Ikeda, N. Sugiyama, B. Pal, G. Marcí, L. Palmisano, H. Noguchi, K. Uosaki, B. Ohtani, Photocatalytic activity of transition-metal-loaded titanium(IV) oxide powders suspended in aqueous solutions: correlation with electron–hole recombination kinetics, Phys. Chem. Chem. Phys. 3 (2001) 267–273.
[14] C. Xiong, K.J. Balkus, Mesoporous molecular sieve derived TiO_2 nanofibers doped with SnO_2, J. Phys. Chem. C 111 (2007) 10359–10367.
[15] J. Liqiang, F. Honggang, W. Baiqi, W. Dejun, X. Baifu, L. Shudan, S. Jiazhong, Effects of Sn dopant on the photoinduced charge property and photocatalytic activity of TiO_2 nanoparticles, Appl. Catal. B 62 (2006) 282–291.
[16] E. Arpaç, F. Sayılkan, M. Asiltürk, P. Tatar, H. Nadir Kiraz, Sayılkan, Photocatalytic performance of Sn-doped and undoped TiO_2 nanostructured thin films under UV and vis-lights, J. Hazard. Mater. 140 (2007) 69–74.
[17] J. Lin, J.C. Yu, D. Lo, S.K. Lam, Photocatalytic activity of rutile $Ti_{1-x}Sn_xO_2$ solid solutions, J. Catal. 183 (1999) 368–372.
[18] D. Li, Y. Xia, Direct fabrication of composite and ceramic hollow nanofibers by electrospinning, Nano Lett. 4 (2004) 933–938.
[19] R. Khan, S.W. Kim, T.-J. Kim, H. Lee, A novel acid–base catalyzed sol–gel synthesis of highly active mesoporous TiO_2 photocatalysts, Bull. Korean Chem. Soc. 28 (2007) 1951–1957.
[20] J.-C. Xu, Y.-L. Shi, J.-E. Huang, B. Wang, H.-L. Li, Doping metal ions only onto the catalyst surface, J. Mol. Catal. A: Chem 219 (2004) 351–355.
[21] I.J. Ochuma, R.P. Fishwich, J. Wood, J.M. Winterbottom, Optimisation of degradation conditions of 1,8-diazabicyclo[5.4.0]undec-7-ene in water and reaction kinetics analysis using a cocurrent downflow contactor photocatalytic reactor, Appl. Catal. B 73 (2007) 259–268.
[22] D. Chen, D. Yang, Q. Wang, Z.Y. Jiang, Effects of boron doping on photocatalytic activity and microstructure of titanium dioxide nanoparticles, Ind. Eng. Chem. Res. 45 (2006) 4110–4116.
[23] C. Adan, A. Bahamonde, M. Fernandez-Garcia, A. Martinez-Arias, Structure and activity of nanosized iron-doped anatase TiO_2 catalysts for phenol photocatalytic degradation, Appl. Catal. B 72 (2007) 11–17.
[24] M. Litter, J. Navío, Photocatalytic properties of iron-doped titania semiconductors, Photochem. Photobiol. A: Chem. 98 (1996) 171–181.
[25] T. Morikawa, Y. Irokawa, T. Ohwaki, Enhanced photocatalytic activity of $TiO_{2-x}N_x$ loaded with copper ions under visible light irradiation, Appl. Catal. A: Gen. 314 (2006) 123–127.
[26] K. Suriye, P. Praserthdam, B. Jongsomjit, Control of Ti^{3+} surface defect on TiO_2 nanocrystal using various calcinations atmosphere as the first step for surface defect creation and its application in photocatalysis, Appl. Surf. Sci. 253 (2007) 3849–3855.